

RESEARCH ARTICLE

Probing interlayer interactions in WSe₂-graphene heterostructures by ultralow-frequency Raman spectroscopy

Yue Liu (刘月), Yu Zhou (周煜), Hao Zhang (张昊), Feirong Ran (冉飞荣),
Weihao Zhao (赵炜昊), Lin Wang (王琳), Chengjie Pei (裴成杰),
Jindong Zhang (张锦东), Xiao Huang (黄晓)[†], Hai Li (李海)[‡]

Key Laboratory of Flexible Electronics (KLOFE) & Institute of Advanced Materials (IAM), Jiangsu National Synergetic Innovation Center for Advanced Materials (SICAM), Nanjing Tech University (NanjingTech), Nanjing 211816, China
Corresponding authors. Email: [†]iamxhuang@njtech.edu.cn, [‡]iamhli@njtech.edu.cn

Received July 20, 2018; accepted August 17, 2018

Interlayer interactions at the heterointerfaces of van der Waals heterostructures (vdWHs), which consist of vertically stacked two-dimensional materials, play important roles in determining their properties. The interlayer interactions are tunable from noncoupling to strong coupling by controlling the twist angle between adjacent layers. However, the influence of stacking sequence and individual component thickness on the properties of vdWHs has rarely been explored. In this work, the influence of the stacking sequence of WSe₂ and graphene in vdWHs of graphene-on-WSe₂ (graphene/WSe₂) or WSe₂-on-graphene (WSe₂/graphene), as well as their thickness, on their interlayer interaction was systematically investigated by ultralow-frequency (ULF) Raman spectroscopy. A series of ULF breathing modes of WSe₂ nanosheets in these vdWHs were observed with frequencies highly dependent on graphene thickness. Interestingly, the ULF breathing modes of WSe₂ red-shifted in graphene/WSe₂ and WSe₂/graphene configurations, and the amount of shift in the former was much larger than that in the latter. In contrast, no obvious ULF shift was observed by varying the twist angle between WSe₂ and graphene. This indicates that the interlayer interaction is more sensitive to the stacking sequence compared with the twist angle. The results provide alternative approaches to modulate the interlayer interaction of vdWHs and, thus, tune their optical and optoelectronic properties.

Keywords interlayer interaction, van der Waals heterostructures, two-dimensional materials, stacking sequence, ultralow-frequency Raman breathing mode

1 Introduction

Recently, much attention has been paid to two-dimensional (2D) vertical heterostructures consisting of two or more kinds of 2D materials vertically stacked through van der Waals (vdW) interactions [1–12]. These van der Waals heterostructures (vdWHs) have showed promising applications in optoelectronics because of their novel excellent optical and electronic properties [1, 3, 4, 7, 9, 13–27]. The combination of 2D materials with various bandgaps broadens their applications in photodetectors, phototransistors, waveguide lasers, mechanical resonators, DNA sequencing, and flexible electronics [28–40]. For instance, a high-performance bipolar phototransistor has been realized based on black phosphorus and transi-

tion metal dichalcogenide (TMDC) heterostructures [28]. A highly sensitive midinfrared photodetector has been achieved based on graphene and Bi₂Se₃ heterostructures at room temperature [41].

It is well known that the interlayer interactions between these 2D materials play important roles in modulating the electrical and optoelectronic properties of vdWHs [1, 3, 4, 11, 14, 16, 18–23, 30, 39, 42–46]. Strong light emission was observed in MoS₂ and WSe₂ heterostructures, in which a new photoluminescence (PL) peak was discovered, indicating the strong interlayer coupling at the heterointerface [4]. Similar interlayer coupling-induced PL peaks were also observed in the heterostructures of WS₂/MoS₂ and MoS₂/MoSe₂/MoS₂ [21, 43]. Moreover, ultrafast charge transfer was discovered in graphene/WSe₂ heterostructures, which was also attributed to the interlayer coupling. It has been reported that interlayer interactions in vdWHs can be tuned from noncoupling to strong coupling by controlling the stacking sequence, twist angle, and component thickness [11, 42, 44, 47, 48]. By altering the stacking se-

*Special Topic: Graphene and other Two-Dimensional Materials (Eds. Daria Andreeva, Wencai Ren, Guangcun Shan & Kostya Novoselov).

quence of mechanically exfoliated graphene and TMDC nanosheets, the electronic properties of heterostructures can be engineered on demand [47, 48]. Tunable interlayer coupling was also realized by stacking chemical vapor deposition (CVD)-grown MoS₂ monolayers at various twist angles [42, 44]. The thickness of the 2D materials also played an important role in determining the interlayer interaction in graphene and MoS₂ heterostructures [11]. To understand the interlayer interactions in vdWHs in detail, it is highly desirable to systematically investigate the effects of stacking sequence and twist angle in combination with the thickness of 2D materials.

The interlayer coupling and stacking order of 2D materials have been investigated by the ultralow-frequency (ULF) Raman spectroscopy [49, 50]. Recently, the ULF Raman spectroscopy has also showed promising ability in characterizing the interfacial interactions in vdWHs [11, 51], which are quite weaker compared with those interactions located at high frequency Raman spectrum.

In this work, the interfacial interaction between WSe₂ and graphene-based vdWHs was systematically investigated by ULF Raman spectroscopy. After single- and few-layer WSe₂ and graphene nanosheets were deposited on SiO₂ substrate by mechanical exfoliation, they were vertically assembled with alternate stacking sequence and various twist angle. With increased graphene thickness, the intrinsic ULF breathing mode of WSe₂ nanosheet was gradually red-shifted. Moreover, new branches of ULF breathing modes were observed as the graphene thickness kept increasing. By altering the stacking sequence of graphene and WSe₂, the ULF breathing modes largely shifted. While the varied twist angle between the graphene and WSe₂ showed much less influence on the ULF breathing mode compared with stacking sequence.

2 Materials and methods

2.1 Materials

Graphite and WSe₂ crystals were bought from HQ Graphene (Netherlands). Silicon oxide wafers were purchased from Bonda Technology. Polymethyl methacrylate (PMMA) was purchased from Aladdin. Dichloromethane was purchased from J&K Scientific Ltd.

2.2 Methods

2.2.1 Fabrication of van der Waals heterostructures

Graphene and WSe₂ nanosheets were firstly deposited on 300 nm SiO₂/Si substrates by mechanical exfoliation. After WSe₂ nanosheet was spin-coated by PMMA (3% wt in dichloromethane), it was transferred onto the pre-deposited graphene by our recently reported clean transfer method under optical microscope [52]. After PMMA film was washed in pure dichloromethane solution at 50°C,

the WSe₂/graphene vdWHs were fabricated. Similarly, the graphene/WSe₂ vdWHs were prepared by stacking graphene onto WSe₂ nanosheets. The vdWHs were annealed in Ar atmosphere at 300°C to enhance the interfacial interaction [11].

2.2.2 Raman characterization

Ultralow-frequency Raman spectroscopy was carried out at room temperature using a micro-Raman spectrometer (LabRAM HR Evolution, Horiba Jobin-Yvon) equipped with a liquid nitrogen-cooled charge-coupled device and a solid state green laser ($\lambda = 532$ nm). A power of ~ 0.2 mW was used to avoid sample heating.

2.2.3 Atomic force microscopy (AFM)

The atomic lattice images of graphene and WSe₂ nanosheets were captured under contact mode by atomic force microscope (MultiMode 8, Bruker) equipped with an E-scanner. Silicon nitride cantilever with the normal spring constant of $0.58 \text{ N}\cdot\text{m}^{-1}$ (DNP-S, Bruker) was used. All images were captured with a scan rate at 10–20 Hz and 256×256 pixel resolution.

3 Results and discussion

As shown in Fig. 1(a), after few-layer WSe₂ was stacked on graphene nanosheet to form the vdWH, ULF Raman spectrometer was employed to investigate the interlayer interaction. Figure 1(b) shows the optical microscopy image of

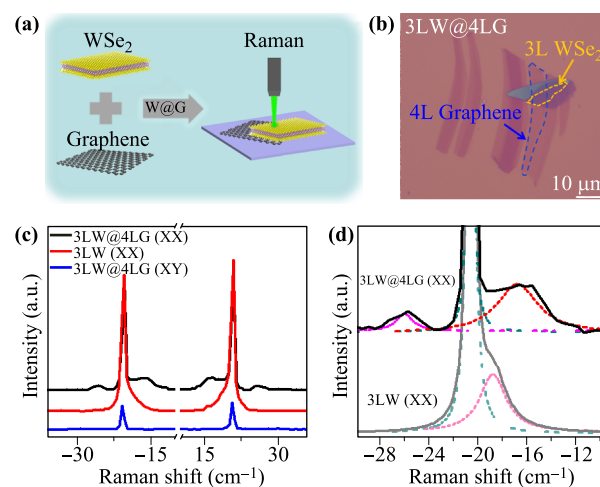


Fig. 1 (a) Schematic illustration for fabricating and characterizing WSe₂/graphene vdWH. (b) Optical image of 3LW/4LG vdWH. The blue and yellow dashed boxes indicated the 4L graphene and 3L WSe₂, respectively. (c) Stokes and anti-Stokes ULF Raman spectra of 3L WSe₂ (red curve) and 3LW/4LG vdWH (black curve), respectively. The blue curve in (c) showed the polarized ULF Raman spectrum of 3LW/4LG vdWH. (d) Anti-Stokes ULF Raman spectra of 3L WSe₂ and 3LW/4LG vdWH after deconvolution, respectively.

3LW/4LG vdWH consisting of three-layer WSe₂ (3LW) and four-layer graphene (4LG) nanosheets, whose thicknesses were identified by optical microscopy (Fig. A1 in Appendix) and further confirmed by Raman spectroscopy [49, 53, 54]. As shown in Fig. 1(d), pristine 3LW has a breathing mode and a shear mode located at -18.8 and -20.6 cm^{-1} in the ULF range [49], respectively. In contrast, 3LW/4LG vdWH shows a shear mode at -20.6 cm^{-1} while two breathing modes at -26.0 and -16.7 cm^{-1} [Fig. 1(d)], respectively, which were confirmed by polarized Raman spectrum [blue curve in Fig. 1(c)]. Similar phenomenon has also been observed in vdWH of 3L MoS₂ on 4L graphene, which was attributed to the interlayer interaction between MoS₂ and graphene nanosheets [11]. Since 4L graphene has no signal in this region, the appearance of two breathing modes should also be arisen from the interlayer interaction between WSe₂ and graphene. Moreover, there is no obvious difference between the Raman spectra of pristine 3LW and 3LW/4LG vdWH in high frequency region (Fig. A2 in Appendix), indicating the interlayer interaction of WSe₂/graphene vdWH could be well probed by ULF Raman spectroscopy.

The influence of graphene thickness on interlayer interaction of WSe₂/graphene vdWH is presented in Fig. 2. As shown in Fig. 2(a), there are three branches of breath-

ing modes in ULF Raman spectra, which are denoted as B1, B2 and B3, respectively. These three breathing modes showed obvious red shift with the increasing thickness of graphene. The B1 peak red-shifted by 0.2 cm^{-1} in 2LW/2LG vdWH compared with that of pristine 2LW. The B2 peak appeared at 34.2 cm^{-1} when 2L WSe₂ was stacked on 3L graphene. It red-shifted by 8.1 cm^{-1} as 2L WSe₂ was stacked on 9L graphene. When 2L WSe₂ was stacked on 7L to 9L graphene, the B2 and B3 peaks simultaneously appeared in 2LW/7LG, 2LW/8LG and 2LW/9LG vdWHs, respectively. Previously, we found that B2 and B3 peaks appeared when 2L MoS₂ (2LM) was stacked on 2L and 5L graphene [11], respectively. It has been reported that graphene has smaller mass per unit area compared to those of TMDCs. New ULF breathing modes of 2LM/*n*LG vdWHs were observed as 2LM was stacked on thick graphene, whose mass per unit area was comparable to that of 2LM [11]. 2LW has larger mass per unit area compared to that of 2LM, thus thicker graphene should be needed to obtain new ULF breathing modes in 2LW/*n*LG vdWHs. As shown in Fig. 2(a), 3L and 7L graphene nanosheets were necessary for generating B2 and B3 peaks in WSe₂/graphene vdWHs, respectively. In addition, no obvious shift was observed for the Raman peaks of 2LW/*n*LG vdWHs located at high frequency range (from 100 cm^{-1} to 500 cm^{-1}) compared to those of 2LW [Figs. 2(b)–(d)], implying the high-frequency Raman modes are insensitive to the interlayer interaction. Moreover, the B2 and B3 peaks of 2LW/9LG were maintained at different temperature (Fig. A3 in Appendix), indicating the interlayer interaction between WSe₂ and graphene was stable.

In order to investigate the stacking sequence dependence of the interlayer interaction, single- to few-layer graphene nanosheets were stacked on 2L WSe₂ nanosheets [Fig. 3(b)], thus the graphene/WSe₂ vdWHs were formed. As shown in Fig. 3(a), there are also three branches of breathing modes (B1', B2' and B3') in ULF Raman spectra of graphene/WSe₂ vdWHs, whose frequencies red-shift with increasing thickness of graphene. There is no obvious difference between B1 and B1' peaks, indicating they are insensitive to the stacking sequence. Similar to the B2 and B3 peaks of WSe₂/graphene vdWHs, B2' and B3' peaks appeared when 3LG and 7LG were stacked on 2L WSe₂ nanosheets, respectively. Similar phenomena were also observed in 4LW/*n*LG vdWHs (Fig. A4 in Appendix). Interestingly, B2' and B3' peaks in graphene/WSe₂ vdWHs show quite larger red shift compared with B2 and B3 peaks in WSe₂/graphene vdWHs [Fig. 3(c)]. As shown in Fig. 3(d), there is almost no difference between the B1 peak of 2LW/2LG and B1' peak of 2LG/2LW. However, the B2' peak of 3LG/2LW red-shifted by 1.6 cm^{-1} compared with the B2 peak of 2LW/3LG. Moreover, the B2' and B3' peaks of 8LG/2LW red-shifted by 0.9 and 1.9 cm^{-1} compared with the B2 and B3 peaks of 2LW/8LG, respectively. It implies that the interlayer interaction be-

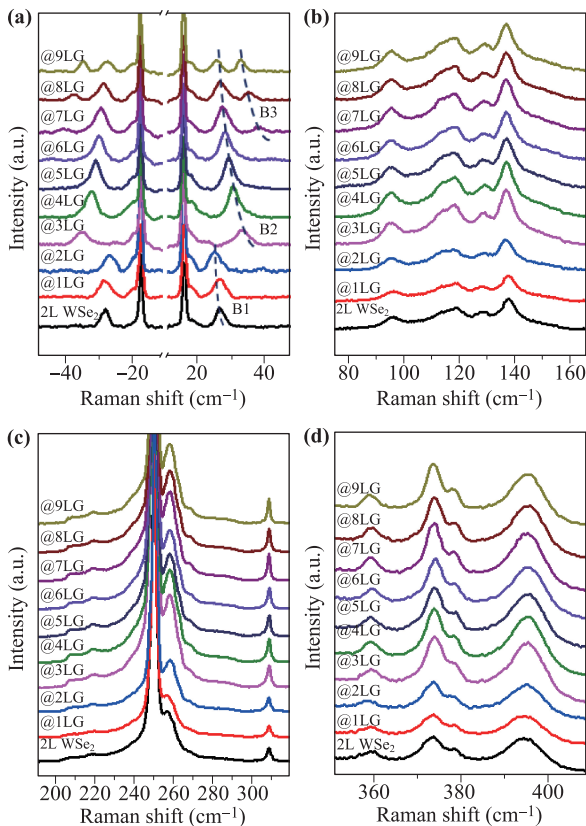


Fig. 2 (a) Stokes and anti-Stokes ULF Raman spectra of heterostructures of 2L WSe₂ on 1–9L graphene. (b–d) Raman spectra of heterostructures of 2L WSe₂ on 1–9L graphene in high frequency region.

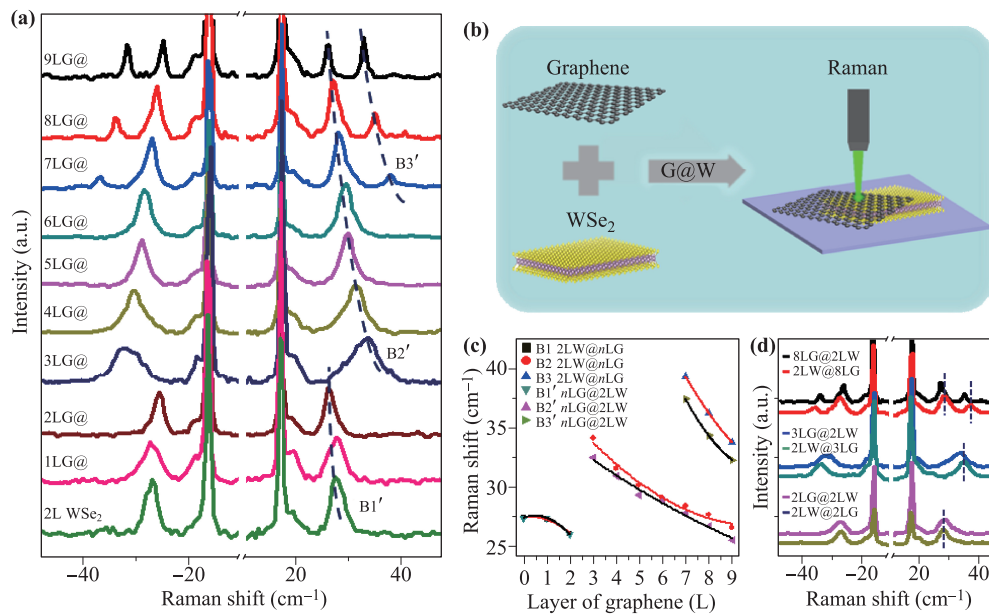


Fig. 3 (a) Stokes and anti-Stokes ULF Raman spectra of heterostructures of 1–9L graphene on 2L WSe₂. (b) Schematic illustration for fabricating and characterizing graphene/WSe₂ vdWH. (c) Stokes Raman shifts of B1, B2 and B3 peaks of 2LW/*n*LG as well as B1', B2' and B3' peaks of *n*LG/2LW as a function of layer number (*n*) of graphene, respectively. (d) Stokes and anti-Stokes ULF Raman spectra of 2LW/2LG, 2LW/3LG, 2LW/8LG, 2LG/2LW, 3LG/2LW, and 8LG/2LW vdWHs, respectively.

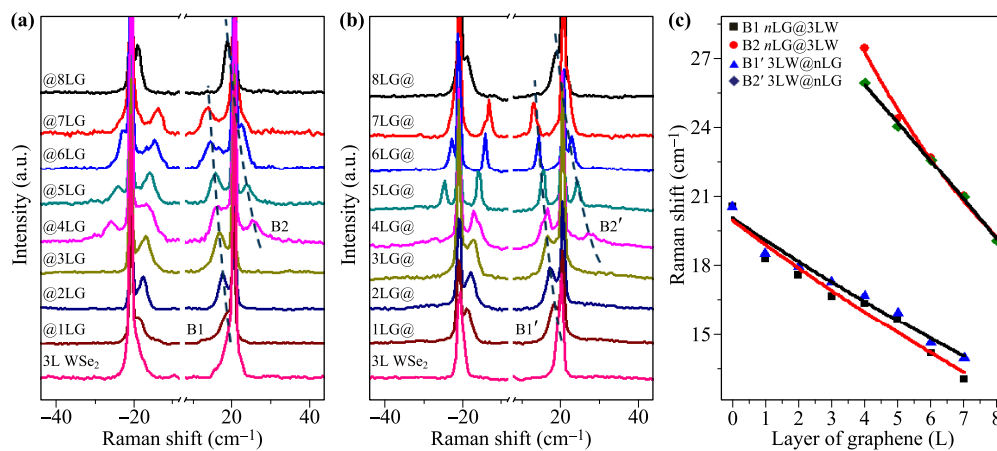


Fig. 4 Stokes and anti-Stokes ULF Raman spectra of heterostructures of (a) 3L WSe₂ on 1–8L graphene and (b) 1–8L graphene on 3L WSe₂, respectively. (c) Stokes Raman shifts of B1 and B2 peaks of 3LW/*n*LG as well as B1' and B2' peaks of *n*LG/3LW as a function of layer number (*n*) of graphene, respectively.

tween 2L WSe₂ and thick graphene nanosheets are sensitive to the stacking sequence. This could be considered as follows. When WSe₂ was stacked on few-layer graphene, the ULF breathing mode red-shifted as well as new breathing modes were generated compared with that of pristine 2LW due to the strong interlayer interaction. In contrast, when few-layer graphene was stacked on 2LW, the ULF breathing mode was affected by not only the interlayer interaction but also the interaction between 2LW and substrate [55, 56]. As shown in Figs. 3(c)–(d), the ULF breathing modes of 2LW/*n*LG were stiffened compared with those of *n*LG/2LW, indicating the interaction between 2LW and SiO₂ substrate softened the ULF breathing modes of *n*LG/2LW.

We further compared the 3LW/*n*LG and *n*LG/3LW vdWHs by ULF Raman spectroscopy. Figs. 4(a)–(b) show the ULF Raman spectra of 3LW/*n*LG and *n*LG/3LW vdWHs, respectively. Both 3LW/*n*LG and *n*LG/3LW vdWHs show similar red-shifted breathing modes with increasing thickness of graphene. The B1' peaks of *n*LG/3LW vdWHs red-shift compared with the B1 peaks

of 3LW/*n*LG vdWHs, which are different from those between 2LW/*n*LG and *n*LG/2LW vdWHs. Although the B2' peaks of 4LG/3LW blue-shifted by 1.5 cm⁻¹ compared with the B2 peak of 3LW/4LG, there is almost no difference between the B2 and B2' peaks after the thickness of graphene exceeded 6L [Fig. 4(c)]. These results indicate that although the interlayer interactions in WSe₂/graphene vdWHs are influenced by stacking sequence, the thickness of WSe₂ might also affect the interaction.

Twist angle has also been reported to play an important role in determining the interlayer coupling of twisted MoS₂ bilayer [42, 44]. However, little is known about its effect on the properties of graphene and TMDCs vdWHs. In order to investigate the role of twist angle in WSe₂ and graphene vdWHs, 2L WSe₂ nanosheets were randomly stacked on 9L graphene to prepare 7 samples of 2LW/9LG vdWHs. Figure 5(a) shows the optical microscopy image of a 2LW/9LG vdWH. The twist angle between WSe₂ and graphene nanosheets were obtained by capturing their atomic lattice images using high-resolution atomic force

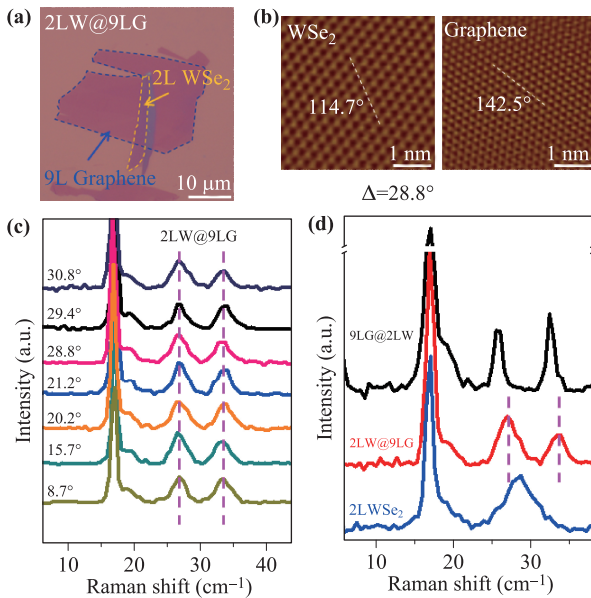


Fig. 5 (a) Optical microscopy image of 2LW/9LG vdWH. (b) Atomic lattice images of WSe₂ and graphene nanosheets shown in (a) captured by high-resolution AFM, respectively. (c) Stokes and anti-Stokes ULF Raman spectra of 7 samples of 2LW/9LG. (d) Anti-Stokes ULF Raman spectra of 9LG/2LW, 2LW/9LG and 2L WSe₂, respectively.

microscopy. As shown in Fig. 5(b), after the atomic lattices of 2L WSe₂ and 9L graphene nanosheets were imaged, the twist angle between them can be measured as 28.8°. The twist angles of other 6 samples of 2LW/9LG vdWHs were also measured by the same method. Figure 5(c) shows the ULF Raman spectra of 2LW/9LG vdWHs with various twist angle. There is no obvious difference among the 7 samples of 2LW/9LG vdWHs regardless of their twist angles. However, the 2LW/9LG vdWH showed much different breathing modes from those of 9LG/2LW

vdWH [Fig. 5(d)], further confirming the interlayer interaction is highly dependent on the stacking sequence.

4 Conclusions

In summary, we found that the stacking sequence of graphene and WSe₂ greatly affected their interlayer interactions in graphene/WSe₂ and WSe₂/graphene vdWHs by using ULF Raman spectroscopy. The graphene thickness also affected the interlayer interaction. The intrinsic ULF breathing mode of WSe₂ was red-shifted and new ULF breathing modes were observed as the graphene thickness increased from 1L to 9L, both in graphene/WSe₂ and WSe₂/graphene vdWHs. Meanwhile, larger amount of shift was found in graphene/WSe₂ vdWHs compared with those in vdWHs with reverse stacking configuration. Moreover, the interlayer interaction was insensitive to the twist angle between WSe₂ and graphene nanosheets. Our results might help to understand the interlayer interaction of vdWHs for modulating their optical and optoelectronic properties.

Acknowledgements This work was supported by the National Natural Science Foundation of China (Grant Nos. 21571101 and 51322202), the Natural Science Foundation of Jiangsu Province in China (Grant Nos. BK20161543 and BK20130927), the Joint Research Fund for Overseas Chinese, Hong Kong and Macao Scholars (Grant No. 51528201), and the Natural Science Foundation of the Jiangsu Higher Education Institutions of China (Grant No. 15KJB430016). Y. Liu acknowledges support by the Graduate Student Scientific Research Innovation Projects in Jiangsu province (Grant No. KYCX17_0950).

Appendix A Supporting information

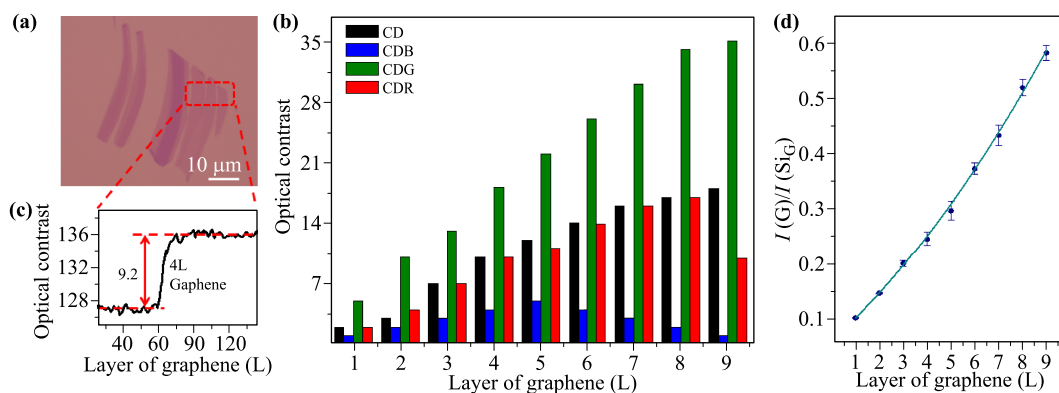


Fig. A1 (a) Optical image of few-layer graphene on 300 nm SiO₂/Si substrate. (b) Plots of optical contrast in color (CD), blue (CDB), green (CDG) and red (CDR) channels of 1L to 9L graphene nanosheets on 300nm SiO₂/Si substrate, respectively. (c) Optical contrast profile in color channel of the red dashed box shown in (a). (d) The experimental and Lorentz fitting of $I(G)/I(Si_G)$ as a function of layer number of 1–9L graphene. The graphene nanosheet marked by red dashed box is 4L from the plot shown in (b). The plot of CD is effective for identifying 1–6L graphene. While 7–9L graphene nanosheets were identified by using the plots of CDB, CDG and CDR.

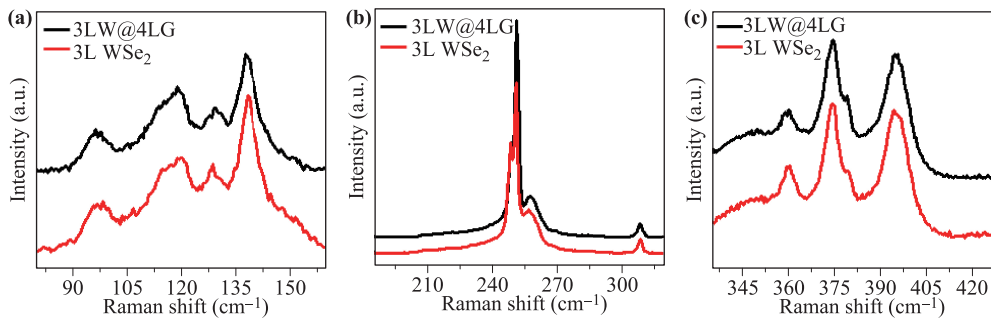


Fig. A2 (a–c) Raman spectra of 3L WSe₂ (red curves) and 3LW/4LG vdWH (black curves) in high frequency range.

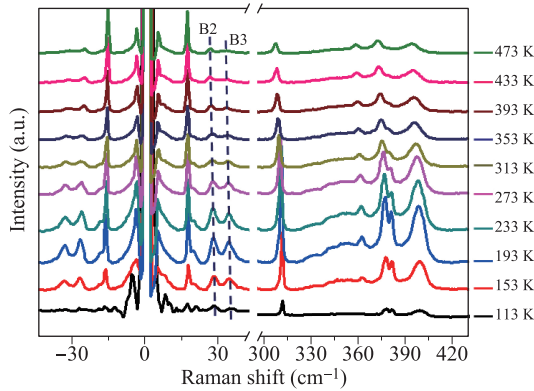


Fig. A3 Raman spectra of 2LW/9LG vdWHs measured in a temperature range from 113 K to 473 K.

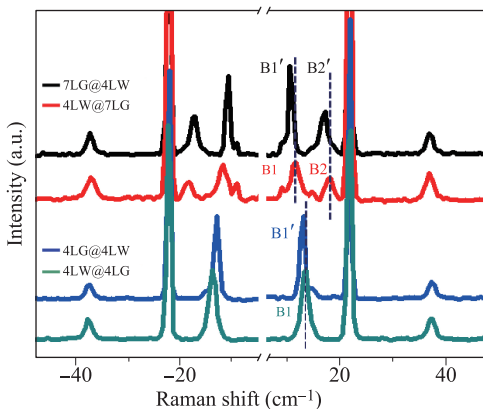


Fig. A4 Stokes and anti-Stokes ULF Raman spectra of heterostructures 4L WSe₂ on 1–8L graphene.

References

1. P. Rivera, J. R. Schaibley, A. M. Jones, J. S. Ross, S. F. Wu, G. Aivazian, P. Klement, K. Seyler, G. Clark, N. J. Ghimire, J. Q. Yan, D. G. Mandrus, W. Yao, and X. D. Xu, Observation of long-lived interlayer excitons in monolayer MoSe₂-WSe₂ heterostructures, *Nat. Commun.* 6(1), 6242 (2015)
2. A. Azizi, S. Eichfeld, G. Geschwind, K. Zhang, B. Jiang, D. Mukherjee, L. Hossain, A. F. Piasecki, B. Kabius, J. A. Robinson, and N. Alem, Freestanding van der Waals heterostructures of graphene and transition metal dichalcogenides, *ACS Nano* 9(5), 4882 (2015)
3. M. H. Chiu, M. Y. Li, W. Zhang, W. T. Hsu, W. H. Chang, M. Terrones, H. Terrones, and L. J. Li, Spectroscopic signatures for interlayer coupling in MoS₂-WSe₂ van der Waals stacking, *ACS Nano* 8(9), 9649 (2014)
4. H. Fang, C. Battaglia, C. Carraro, S. Nemsak, B. Ozdol, J. S. Kang, H. A. Bechtel, S. B. Desai, F. Kronast, A. A. Unal, G. Conti, C. Conlon, G. K. Palsson, M. C. Martin, A. M. Minor, C. S. Fadley, E. Yablonovitch, R. Maboudian, and A. Javey, Strong interlayer coupling in van der Waals heterostructures built from single-layer chalcogenides, *Proc. Natl. Acad. Sci. USA* 111(17), 6198 (2014)
5. A. Nourbakhsh, A. Zubair, M. S. Dresselhaus, and T. Palacios, Transport properties of a MoS₂/WSe₂ heterojunction transistor and its potential for application, *Nano Lett.* 16(2), 1359 (2016)
6. J. H. Yu, H. R. Lee, S. S. Hong, D. Kong, H. W. Lee, H. Wang, F. Xiong, S. Wang, and Y. Cui, Vertical heterostructure of two-dimensional MoS₂ and WSe₂ with vertically aligned layers, *Nano Lett.* 15(2), 1031 (2015)
7. C. H. Lee, G. H. Lee, A. M. van der Zande, W. Chen, Y. Li, M. Han, X. Cui, G. Arefe, C. Nuckolls, T. F. Heinz, J. Guo, J. Hone, and P. Kim, Atomically thin p-n junctions with van der Waals heterointerfaces, *Nat. Nanotechnol.* 9(9), 676 (2014)
8. L. Britnell, R. V. Gorbachev, R. Jalil, B. D. Belle, F. Schedin, A. Mishchenko, T. Georgiou, M. I. Katsnelson, L. Eaves, S. V. Morozov, N. M. Peres, J. Leist, A. K. Geim, K. S. Novoselov, and L. A. Ponomarenko, Field-effect tunneling transistor based on vertical graphene heterostructures, *Science* 335(6071), 947 (2012)
9. W. J. Yu, Y. Liu, H. Zhou, A. Yin, Z. Li, Y. Huang, and X. Duan, Highly efficient gate-tunable photocurrent generation in vertical heterostructures of layered materials, *Nat. Nanotechnol.* 8(12), 952 (2013)
10. H. Xu, J. Wu, Q. Feng, N. Mao, C. Wang, and J. Zhang, High responsivity and gate tunable graphene-MoS₂ hybrid phototransistor, *Small* 10(11), 2300 (2014)
11. H. Li, J. B. Wu, F. Ran, M. L. Lin, X. L. Liu, Y. Zhao, X. Lu, Q. Xiong, J. Zhang, W. Huang, H. Zhang, and P. H. Tan, Interfacial interactions in van der Waals heterostructures of MoS₂ and graphene, *ACS Nano* 11(11), 11714 (2017)

12. Y. C. Lin, C. Y. Chang, R. K. Ghosh, J. Li, H. Zhu, R. Addou, B. Diaconescu, T. Ohta, X. Peng, N. Lu, M. J. Kim, J. T. Robinson, R. M. Wallace, T. S. Mayer, S. Datta, L. J. Li, and J. A. Robinson, Atomically thin heterostructures based on single-layer tungsten diselenide and graphene, *Nano Lett.* 14(12), 6936 (2014)
13. Q. Z. Li, L. P. Tang, C. X. Zhang, D. Wang, Q. J. Chen, Y. X. Feng, L. M. Tang, and K. Q. Chen, Seeking the dirac cones in the MoS₂/WSe₂ van der Waals heterostructure, *Appl. Phys. Lett.* 111(17), 171602 (2017)
14. F. Ullah, Y. Sim, C. T. Le, M. J. Seong, J. I. Jang, S. H. Rhim, B. C. Tran Khac, K. H. Chung, K. Park, Y. Lee, K. Kim, H. Y. Jeong, and Y. S. Kim, Growth and simultaneous valleys manipulation of two-dimensional MoSe₂-WSe₂ lateral heterostructure, *ACS Nano* 11(9), 8822 (2017)
15. C. Chakraborty, L. Y. Qiu, K. Konthasinghe, A. Mukherjee, S. Dhara, and N. Vamivakas, 3D Localized Trions in Monolayer WSe₂ in a Charge Tunable van der Waals Heterostructure, *Nano Lett.* 18(5), 2859 (2018)
16. K. W. Tang, W. H. Qi, Y. J. Li, and T. R. Wang, Electronic properties of van der Waals heterostructure of black phosphorus and MoS₂, *J. Phys. Chem. C* 122(12), 7027 (2018)
17. J. G. Roch, N. Leisgang, G. Froehlicher, P. Makk, K. Watanabe, T. Taniguchi, C. Schonberger, and R. J. Warburton, Quantum-confined stark effect in a MoS₂ monolayer van der Waals heterostructure, *Nano Lett.* 18(2), 1070 (2018)
18. M. Okada, A. Kutana, Y. Kureishi, Y. Kobayashi, Y. Saito, T. Saito, K. Watanabe, T. Taniguchi, S. Gupta, Y. Miyata, B. I. Yakobson, H. Shinohara, and R. Kitaura, Direct and indirect interlayer excitons in a van der Waals heterostructure of hBN/WS₂/MoS₂/hBN, *ACS Nano* 12(3), 2498 (2018)
19. X. R. Hu, J. M. Zheng, and Z. Y. Ren, Strong interlayer coupling in phosphorene/graphene van der Waals heterostructure: A first-principles investigation, *Front. Phys.* 13(2), 137302 (2018)
20. A. T. Hanbicki, H. J. Chuang, M. R. Rosenberger, C. S. Hellberg, S. V. Sivaram, K. M. McCreary, I. I. Mazin, and B. T. Jonker, Double indirect interlayer exciton in a MoSe₂/WSe₂ van der Waals heterostructure, *ACS Nano* 12(5), 4719 (2018)
21. T. Deilmann and K. S. Thygesen, Interlayer trions in the MoS₂/WS₂ van der Waals heterostructure, *Nano Lett.* 18(2), 1460 (2018)
22. H. Yuan and Z. Li, Interfacial properties of black phosphorus/transition metal carbide van der Waals heterostructures, *Front. Phys.* 13(3), 138103 (2018)
23. Z. Z. Yan, Z. H. Jiang, J. P. Lu, and Z. H. Ni, Interfacial charge transfer in WS₂ monolayer/CsPbBr₃ microplate heterostructure, *Front. Phys.* 13(4), 138115 (2018)
24. T. C. Song, X. H. Cai, M. W. Y. Tu, X. O. Zhang, B. V. Huang, N. P. Wilson, K. L. Seyler, L. Zhu, T. Taniguchi, K. Watanabe, M. A. McGuire, D. H. Cobden, D. Xiao, W. Yao, and X. D. Xu, Giant tunneling magnetoresistance in spin-filter van der Waals heterostructures, *Science* 360(6394), 1214 (2018)
25. R. Cheng, F. Wang, L. Yin, Z. Wang, Y. Wen, T. A. Shifa, and J. He, High-performance, multifunctional devices based on asymmetric van der Waals heterostructures, *Nat. Electron.* 1(6), 356 (2018)
26. X. W. Zhang, D. W. He, J. Q. He, S. Q. Zhao, S. C. Hao, Y. S. Wang, and L. X. Yi, Ultrafast interlayer photocarrier transfer in graphene-MoSe₂ van der Waals heterostructure, *Chin. Phys. B* 26(9), 097202(2017)
27. Y. Chen, Z. X. Fan, Z. C. Zhang, W. X. Niu, C. L. Li, N. L. Yang, B. Chen, and H. Zhang, Two-dimensional metal nanomaterials: Synthesis, properties, and applications, *Chem. Rev.* 118(13), 6409 (2018)
28. H. Li, L. Ye, and J. B. Xu, High-performance broadband floating-base bipolar phototransistor based on WSe₂/BP/MoS₂ heterostructure, *ACS Photon.* 4(4), 823 (2017)
29. Z. Q. Li, C. Cheng, N. N. Dong, C. Romero, Q. M. Lu, J. Wang, J. R. V. de Aldana, Y. Tan, and F. Chen, Q-switching of waveguide lasers based on graphene/WS₂ van der Waals heterostructure, *Photon. Res.* 5(5), 406 (2017)
30. Y. Liu, B. N. Shivananju, Y. S. Wang, Y. P. Zhang, W. Z. Yu, S. Xiao, T. Sun, W. L. Ma, H. R. Mu, S. H. Lin, H. Zhang, Y. R. Lu, C. W. Qiu, S. J. Li, and Q. L. Bao, Highly efficient and air-stable infrared photodetector based on 2D layered graphene-black phosphorus heterostructure, *ACS Appl. Mater. Interfaces* 9(41), 36137 (2017)
31. M. Will, M. Hamer, M. Muller, A. Noury, P. Weber, A. Bachtold, R. V. Gorbachev, C. Stampfer, and J. Guttinger, High quality factor graphene-based two-dimensional heterostructure mechanical resonator, *Nano Lett.* 17(10), 5950 (2017)
32. X. Yan, C. S. Liu, C. Li, W. Z. Bao, S. J. Ding, D. W. Zhang, and P. Zhou, Tunable SnSe₂/WSe₂ heterostructure tunneling field effect transistor, *Small* 13(34), 1701478 (2017)
33. L. Ye, P. Wang, W. J. Luo, F. Gong, L. Liao, T. D. Liu, L. Tong, J. F. Zang, J. B. Xu, and W. D. Hu, Highly polarization sensitive infrared photodetector based on black phosphorus-on-WSe₂ photogate vertical heterostructure, *Nano Energy* 37(37), 53 (2017)
34. W. Z. Yu, S. J. Li, Y. P. Zhang, W. L. Ma, T. Sun, J. Yuan, K. Fu, and Q. L. Bao, Near-infrared photodetectors based on MoTe₂/graphene heterostructure with high responsivity and flexibility, *Small* 13(24), 1700268 (2017)
35. K. Zhang, X. Fang, Y. L. Wang, Y. Wan, Q. J. Song, W. H. Zhai, Y. P. Li, G. Z. Ran, Y. Ye, and L. Dai, Ultrasensitive near-infrared photodetectors based on a graphene-MoTe₂-graphene vertical van der Waals heterostructure, *ACS Appl. Mater. Interfaces* 9(6), 5392 (2017)
36. Y. Chen, X. D. Wang, G. J. Wu, Z. Wang, H. H. Fang, T. Lin, S. Sun, H. Shen, W. D. Hu, J. L. Wang, J. L. Sun, X. J. Meng, and J. H. Chu, High-performance photovoltaic detector based on MoTe₂/MoS₂ van der Waals heterostructure, *Small* 14(9), 1703293 (2018)

37. B. Q. Luan, and R. H. Zhou, Spontaneous transport of single-stranded DNA through graphene-MoS₂ heterostructure nanopores, *ACS Nano* 12(4), 3886 (2018)
38. H. Xu, X. Y. Han, X. Dai, W. Liu, J. Wu, J. T. Zhu, D. Y. Kim, G. F. Zou, K. A. Sablon, A. Sergeev, Z. Guo, and H. Liu, SK. A. Ablon, A. Sergeev, Z. X. Guo and H. Y. Liu, High detectivity and transparent few-layer MoS₂/glassy-graphene heterostructure photodetectors, *Adv. Mater.* 30(13), 1706561 (2018)
39. Y. Tan, X. B. Liu, Z. L. He, Y. R. Liu, M. W. Zhao, H. Zhang, and F. Chen, Tuning of interlayer coupling in large-area graphene/WSe₂ van der Waals heterostructure via ion irradiation: Optical evidences and photonic applications, *ACS Photon.* 4(6), 1531 (2017)
40. X. Huang, Ch. L. Tan, Z. Y. Yin, and H. Zhang, Hybrid nanostructures based on two-dimensional nanomaterials, *Adv. Mater.* 26(14), 2185 (2014)
41. J. Kim, V. Park, H. Jang, N. Koirala, J. B. Lee, U. J. Kim, H. S. Lee, Y. G. Roh, H. Lee, S. Sim, S. Cha, C. In, J. Park, J. Lee, M. Noh, J. Moon, M. Salehi, J. Sung, S. S. Chee, M. H. Ham, M. H. Jo, S. Oh, J. H. Ahn, S. W. Hwang, D. Kim, and H. Choi, Highly sensitive, gate-tunable, room-temperature mid-infrared photodetection based on graphene-Bi₂Se₃ heterostructure, *ACS Photon.* 4(3), 482 (2017)
42. K. Liu, L. Zhang, T. Cao, C. Jin, D. Qiu, Q. Zhou, A. Zettl, P. Yang, S. G. Louie, and F. Wang, Evolution of interlayer coupling in twisted molybdenum disulfide bilayers, *Nat. Commun.* 5(1), 4966 (2014)
43. M. Baranowski, A. Surrente, L. Kłopotowski, J. M. Urban, N. Zhang, D. K. Maude, K. Wiwatowski, S. Mackowski, Y. C. Kung, D. Dumcenco, A. Kis, and P. Plochocka, Probing the interlayer exciton physics in a MoS₂/MoSe₂/MoS₂ van der Waals heterostructure, *Nano Lett.* 17(10), 6360 (2017)
44. S. Huang, X. Ling, L. Liang, J. Kong, H. Terrones, V. Meunier, and M. S. Dresselhaus, Probing the interlayer coupling of twisted bilayer MoS₂ using photoluminescence spectroscopy, *Nano Lett.* 14(10), 5500 (2014)
45. W. Yao, E. Wang, C. Bao, Y. Zhang, K. Zhang, K. Bao, C. K. Chan, C. Chen, J. Avila, M. C. Asensio, J. Zhu, and S. Zhou, Quasicrystalline 30° twisted bilayer graphene as an incommensurate superlattice with strong interlayer coupling, *Proc. Natl. Acad. Sci. USA* 115(27), 6928 (2018)
46. H. Zhang, Ultrathin two-dimensional nanomaterials, *ACS Nano* 9(10), 9451 (2015)
47. M. S. Choi, G. H. Lee, Y. J. Yu, D. Y. Lee, S. H. Lee, P. Kim, J. Hone, and W. J. Yoo, Controlled charge trapping by molybdenum disulfide and graphene in ultrathin heterostructured memory devices, *Nat. Commun.* 4(1), 1624 (2013)
48. K. Kim, S. Larentis, B. Fallahazad, K. Lee, J. Xue, D. C. Dillen, C. M. Corbet, and E. Tutuc, Band alignment in WSe₂-graphene heterostructures, *ACS Nano* 9(4), 4527 (2015)
49. Y. Zhao, X. Luo, H. Li, J. Zhang, P. T. Araujo, C. K. Gan, J. Wu, H. Zhang, S. Y. Quek, M. S. Dresselhaus, and Q. Xiong, Interlayer breathing and shear modes in few-trilayer MoS₂ and WSe₂, *Nano Lett.* 13(3), 1007 (2013)
50. R. He, J. A. Yan, Z. Yin, Z. Ye, G. Ye, J. Cheng, J. Li, and C. H. Lui, Coupling and stacking order of ReS₂ atomic layers revealed by ultralow-frequency Raman spectroscopy, *Nano Lett.* 16(2), 1404 (2016)
51. S. Huang, L. Liang, X. Ling, A. A. Puretzky, D. B. Geoghegan, B. G. Sumpter, J. Kong, V. Meunier, and M. S. Dresselhaus, Low-frequency interlayer Raman modes to probe interface of twisted bilayer MoS₂, *Nano Lett.* 16(2), 1435 (2016)
52. H. Li, J. Wu, X. Huang, Z. Yin, J. Liu, and H. Zhang, A universal, rapid method for clean transfer of nanostructures onto various substrates, *ACS Nano* 8(7), 6563 (2014)
53. H. Li, J. Wu, X. Huang, G. Lu, J. Yang, X. Lu, Q. Xiong, and H. Zhang, Rapid and reliable thickness identification of two-dimensional nanosheets using optical microscopy, *ACS Nano* 7(11), 10344 (2013)
54. X. L. Li, X. F. Qiao, W. P. Han, Y. Lu, Q. H. Tan, X. L. Liu, and P. H. Tan, Layer number identification of intrinsic and defective multilayered graphenes up to 100 layers by the Raman mode intensity from substrates, *Nanoscale* 7(17), 8135 (2015)
55. M. Buscema, G. A. Steele, H. S. J. van der Zant, and A. Castellanos-Gomez, The effect of the substrate on the Raman and photoluminescence emission of single-layer MoS₂, *Nano Res.* 7(4), 561 (2014)
56. S. Wu, X. Shi, Y. Liu, L. Wang, J. Zhang, W. Zhao, P. Wei, W. Huang, X. Huang, and H. Li, The influence of two-dimensional organic adlayer thickness on the ultralow frequency Raman spectra of transition metal dichalcogenide nanosheets, *Sci. China Mater.* (2018), doi: 10.1007/s40843-018-9303-6